Theor Chem Acc (2012) 131:1181
DOI 10.1007/s00214-012-1181-3

REGULAR ARTICLE

Franck–Condon factors in curvilinear coordinates: the photoelectron spectrum of ammonia

Amedeo Capobianco · Raffaele Borrelli · Canio Noce · Andrea Peluso

Received: 1 November 2011 / Accepted: 3 February 2012 / Published online: 2 March 2012

Abstract An approach to the calculation of Franck–Condon factors in curvilinear coordinates is outlined. The approach is based on curvilinear normal coordinates, which allows for an easy extension of Duschinsky's transformation to the case of curvilinear coordinates, and on the power series expansion of the kinetic energy operator. Its usefulness in the case of molecules undergoing large displacements of their equilibrium nuclear configurations upon excitation is then demonstrated by an application to the vibrational structure of the photoelectron spectrum of ammonia, using an anharmonic potential only for the symmetric stretching and bending coordinates of the radical cation.

Keywords Franck–Condon factors · Curvilinear coordinates · Photoelectron spectra

1 Introduction

Ammonia is a very interesting molecule for spectroscopists and theoreticians. In the ground electronic state, it exhibits two distinct equilibrium nuclear configurations that, by interconverting each other along the large amplitude motion, the so-called umbrella motion, cause the splitting of the rovibrational energy levels. Furthermore, ammonia undergoes significantly large displacements of its equilibrium nuclear geometry upon excitation and photoionization, which reflect into broad absorption bands, with a well-resolved vibrational and rovibrational structure, as shown in Fig. 1 for the $\tilde{X}^2A_2'' \leftarrow \tilde{X}^1A_1'$ transition. The analyses of both the vibrational pattern [1] and of the rotational fine structure of some vibronic peaks [2] of the UV absorption band occurring at 217 nm have led to the conclusion that the excited electronic state has a planar equilibrium nuclear configuration, belonging to D_{3h} point group. A very similar vibrational pattern has also been observed in the lower-energy region of its photoelectron spectrum, leading to the conclusion that even the $\tilde{X}^2A_2''$ ionic state is planar [3–5].

Both the splitting of the energy levels of the rovibrational spectrum and the well-resolved vibrational pattern of the electronic and photoelectronic spectra provide important experimental data for theoreticians involved in the application of sophisticated theoretical models for treating strong anharmonic effects [6, 7], and in the development of efficient methodologies for the calculations of spectroscopic band shapes, that is, Franck–Condon (FC) factors. It is indeed well-known that in the case an electronic transition takes place between two electronic states exhibiting a large displacement of their equilibrium positions, the calculation of the FC factors may pose problems, especially when the Cartesian representation of normal modes and the harmonic approximation are adopted [8, 9]. In fact, in rectilinear coordinates, a large displacement along a bending coordinate always implies a motion along the two bond distances of the angular coordinate, Fig. 2, so that on carrying out the projection of the normal modes of one

Dedicated to Professor Vincenzo Barone and published as part of the special collection of articles celebrating his 60th birthday.

A. Capobianco · C. Noce
Dipartimento di Fisica E.R. Caianiello, Università di Salerno, Via Ponte don Melillo, 84084 Fisciano, SA, Italy

R. Borrelli · A. Peluso (✉)
Dipartimento di Chimica e Biologia, Università di Salerno, Via Ponte don Melillo, 84084 Fisciano, SA, Italy
e-mail: apeluso@unisa.it

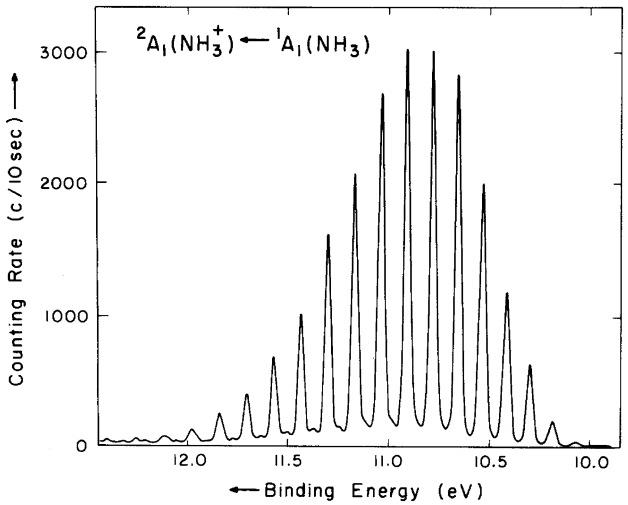

Fig. 1 The lowest energy band of the photoelectron spectrum of ammonia, reproduced with permission from Rabalais et al. [5]

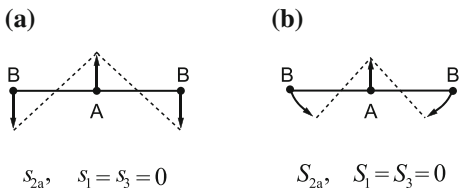

Fig. 2 Representations of the bending motion (at arbitrary low speed) in rectilinear (**a**) and curvilinear (**b**) coordinates for the linear molecule AB_2. *S* denotes curvilinear coordinates, *s* rectilinear ones

electronic state onto those of the other—the Duschinsky's transformation—those stretching modes come out to be significantly displaced, causing the appearance in the computed spectrum of several vibrational progressions, due to excitations of both the large amplitude and the stretching modes, which have no counterparts in the observed spectrum [9, 10].

The most successful attempts to rationalize the photoelectron spectrum of ammonia through the computation of Franck–Condon factors was based on procedures that overcome Duschinsky's transformation, avoiding the use of normal modes of both electronic states [11–14]. Recently, a very satisfying reproduction of the photoelectron spectrum of ammonia, based on Duschinsky's transformation and the Cartesian representation of the normal coordinates, has been obtained by using a two-dimensional approach, including the symmetric stretching and bending coordinates. A high-order polynomial for describing the strong anharmonic couplings between the two modes was necessary for correcting the spurious displacement of the symmetric stretching mode predicted by Duschinsky's transformation in the Cartesian representation of the normal modes [10], which causes the appearance in the computed spectrum of vibrational progressions that are not present in the observed one. The adopted methodology is therefore quite cumbersome, requiring the knowledge of the potential energy of NH_3^+ on a large grid of nuclear coordinates. In the present work, with the aim of setting up an easier and general procedure to compute the FC factors for floppy molecules, those undergoing large displacements of their equilibrium positions upon light excitation, we afford the computation of the ammonia photoelectron spectrum by using curvilinear coordinates, with the hope of relieving the high computational effort of computing anharmonic potential energy terms. Because our main interest is in finding out practical ways for computing FC factors for difficult cases, anharmonic terms in the potential energy expression have been considered only for the two vibrational coordinates, the symmetric stretching and bending, which in the photoelectron spectrum of ammonia play a predominant role.

2 Theoretical approach

Curvilinear internal coordinates such as bond elongations (stretching) or variations of valence angles (bending) are potentially the best suited to treat molecular vibrations [15]. Figure 2 gives the classical description of the bending motion for an AB_2 linear molecule [16], both in linearized internal coordinates (a) and in true curvilinear internal coordinates (b). In curvilinear coordinates, nuclei are allowed to follow curved trajectories, whereas linearized internal coordinates force nuclear motion along straight lines, defined by the projections of the exact internal coordinates onto fixed Cartesian axes. A linearized internal coordinate s_j coincides with the curvilinear one S_j in the limit of infinitesimal displacements of atoms from their equilibrium positions. Therefore, in the range of validity of the harmonic approximation, there is no distinction between linear and curvilinear coordinates, but when large displacements are involved, such as those observed in going from the equilibrium geometry of NH_3 to that of NH_3^+, the two sets of coordinates are no longer equivalent. In the example of Fig. 2, the motion along a linearized bending coordinate involves an elongation of the A-B bond. Even if the potential energy was strictly quadratic in curvilinear coordinates, anharmonic terms would be needed in the rectilinear representation to obtain an equivalent description of the nuclear motion [17]. Of course, both the rectilinear and the curvilinear representation must lead to identical results when an exact treatment of the vibrational problem is carried out, but they yield different results at lower orders of approximation. In particular, the expression of the potential energy in curvilinear coordinates is generally simpler than that obtained by adopting rectilinear coordinates [16–18], but the linear momentum and the

kinetic energy operators in curvilinear coordinates are much more involved [19–22].

The quantum vibrational Hamiltonian in curvilinear coordinate is [19]:

$$\hat{H}_S = -\frac{\hbar^2}{2} G^{1/4} \left(\frac{\partial}{\partial \mathbf{S}}\right)^T G^{-1/2} \mathbf{G} \left(\frac{\partial}{\partial \mathbf{S}}\right) G^{1/4} + V, \tag{1}$$

where $\mathbf{S}$ is the column vector of curvilinear internal coordinates, V is the potential energy, $\mathbf{G}$ and G are the metric matrix and its determinant, respectively, both depending on $\mathbf{S}$. The subscript S in the operator indicates normalization with respect to the $\mathbf{S}$ coordinates and the superscript T denotes transposition. By performing the differentiation, Eq. 1 can be rewritten as:

$$\hat{H}_S = -\frac{\hbar^2}{2} \sum_{j,k} \frac{\partial}{\partial S_j} G_{jk}(S) \frac{\partial}{\partial S_k} + V(S) + V_{\text{kin}}(S), \tag{2}$$

where

$$V_{\text{kin}} = \frac{5\hbar^2}{32G^2} \sum_{j,k} G_{jk} \frac{\partial G}{\partial S_j} \frac{\partial G}{\partial S_k} - \frac{\hbar^2}{8G} \sum_{j,k} \frac{\partial G_{jk}}{\partial S_j} \frac{\partial G}{\partial S_k} - \frac{\hbar^2}{8G} \sum_{j,k} G_{jk} \frac{\partial^2 G}{\partial S_j \partial S_k} \tag{3}$$

collects the terms of the kinetic energy operator which depend only on coordinates, thus acting like a potential energy term. The easiest way of taking properly into account the dependence of G_{jk} on $\mathbf{S}$ coordinates is that of expanding them into a power series. That yields:

$$\hat{H}_S = -\frac{\hbar^2}{2} \left(\sum_{j,k} G^0_{jk} \frac{\partial^2}{\partial S_j \partial S_k} + \sum_{j,k,\ell} G'_{jk\ell} \frac{\partial}{\partial S_j} S_\ell \frac{\partial}{\partial S_k} + \frac{1}{2} \sum_{j,k,\ell,m} G''_{jk\ell m} \frac{\partial}{\partial S_j} S_\ell S_m \frac{\partial}{\partial S_k} + \cdots \right) + V_{\text{kin}}(S) + V(S) \tag{4}$$

where

$$G^0_{jk} = G_{jk}(0) \tag{5}$$

$$G'_{jk\ell} = \left(\frac{\partial G_{jk}}{\partial S_\ell}\right)_0; \tag{6}$$

$$G''_{jk\ell m} = \left(\frac{\partial^2 G_{jk}}{\partial S_\ell \partial S_m}\right)_0. \tag{7}$$

The Hamiltonian in Eq. 4 can be cast into a more manageable form by introducing curvilinear normal coordinates [18, 19, 23–26]. First, the so-called linearized internal coordinates, which are linear combinations of Cartesian displacements [15, 27, 28], are introduced:

$$\mathbf{s} = \mathbf{B}_0 \boldsymbol{\sigma}, \tag{8}$$

where $\mathbf{s}$ and $\boldsymbol{\sigma}$ are the column vectors of the linearized internal and the Cartesian displacement coordinates, respectively, and $\mathbf{B}_0$ is the Jacobian matrix whose elements depend only on the equilibrium geometry of the molecule. Normal coordinates $\mathbf{Q}$ are linear combinations of linearized internal coordinates:

$$\mathbf{s} = \mathbf{L}_0 \mathbf{Q}, \tag{9}$$

in which:

$$\mathbf{L}_0 = \frac{\partial \mathbf{s}}{\partial \mathbf{Q}} = \mathbf{B}_0 \mathbf{M}^{-1/2} \mathbf{L}, \tag{10}$$

where $\mathbf{M}$ is the diagonal matrix of atomic masses and $\mathcal{L}$ is the normalized matrix of normal modes in Cartesian coordinates, whose elements are not a function of the coordinates. The linear relationship between $\mathbf{Q}$ and $\mathbf{s}$ ensures that the elements of matrix of the effective masses:

$$\mathbf{G}^0 = \mathbf{L}_0 \mathbf{L}_0^T, \tag{11}$$

do not depend on the coordinates $\mathbf{s}$.

Then, "curvilinear normal coordinates" $\bar{\mathbf{Q}}$, defined as:

$$\mathbf{S} = \mathbf{L}_0 \bar{\mathbf{Q}}, \tag{12}$$

are introduced so that the vibrational Hamiltonian Eq. 2 assumes the form:

$$\hat{H} = -\frac{\hbar^2}{2} \sum_{r,s} \frac{\partial}{\partial \bar{Q}_r} g_{rs}(\bar{Q}) \frac{\partial}{\partial \bar{Q}_s} + V(\bar{Q}) + V_{\text{kin}}(\bar{Q}), \tag{13}$$

where

$$\mathbf{g} = \mathbf{R}^T \mathbf{G} \mathbf{R}; \quad \mathbf{R} = \left(\mathbf{L}_0^{-1}\right)^T. \tag{14}$$

In the limit of infinitesimal vibrational amplitudes, curvilinear internal coordinates coincide with linearized ones; therefore, (Eqs. 9, 12) curvilinear normal coordinates coincide with the linear ones. This in turn implies that (1) $\mathbf{g}^0$, that is, the metric matrix over curvilinear normal coordinates at the zero order of expansion, coincides with the unit matrix and (2) anharmonic terms vanish in the potential energy expressed as a function of $\bar{Q}$. Therefore, for finite amplitudes, a power series expansion provides a kinetic energy operator of the form:

$$\hat{T} = -\frac{\hbar^2}{2} \sum_r \frac{\partial^2}{\partial \bar{Q}_r{}^2} + \Delta\hat{T} + V_{\text{kin}}. \tag{15}$$

$\Delta\hat{T}$ and V_{kin} being the kinetic energy terms originated by the curvilinear nature of $\bar{Q}$:

$$\Delta\hat{T}\left(\bar{Q}, \frac{\partial}{\partial \bar{Q}}\right) = -\frac{\hbar^2}{2} \left(\sum_{r,s,t} g'_{rst} \frac{\partial}{\partial \bar{Q}_r} \bar{Q}_t \frac{\partial}{\partial \bar{Q}_s} + \frac{1}{2} \sum_{r,s,t,u} g''_{rstu} \frac{\partial}{\partial \bar{Q}_r} \bar{Q}_t \bar{Q}_u \frac{\partial}{\partial \bar{Q}_s} + \cdots \right), \tag{16}$$

where, as before (Eq. 6) [26]:

$$g'_{rst} = \left(\frac{\partial g_{rs}}{\partial \bar{Q}_t}\right)_0 = \sum_{j,k,l} G'_{jk\ell} R_{jr} R_{ks} L^0_{\ell t}; \quad \text{etc.} \tag{17}$$

and a potential energy in the form:

$$V = 2\pi^2 c^2 \sum_r \tilde{\nu}_r^2 \bar{Q}_r^2 + \Delta V(\bar{Q}) \tag{18}$$

where ΔV collects the anharmonic terms of the potential and $\tilde{\nu}_r$ are the harmonic frequencies expressed as wavenumbers. Combining Eqs. 15 and 18, the vibrational Hamiltonian may be written as:

$$\hat{H} = \hat{H}_0 + \Delta\hat{T} + \Delta V + V_{\text{kin}}, \tag{19}$$

where $\hat{H}_0$ is the harmonic Hamiltonian:

$$\hat{H}_0 = -\frac{\hbar^2}{2} \sum_r \frac{\partial}{\partial \bar{Q}_r^2} + 2\pi^2 c^2 \sum_r \tilde{\nu}_r^2 \bar{Q}_r^2, \tag{20}$$

Approximate eigenfunctions of $\hat{H}$ can be obtained by means of perturbation theory [29] or variational method, using the basis set of the eigenfunctions of $\hat{H}_0$.

Although both $\bar{\mathbf{Q}}$ and $\mathbf{S}$ are curvilinear coordinates, they are linearly related (Eq. 12), this is the key-point for the extension of Duschinsky's transformation [30] in curvilinear normal coordinates. Reminding that internal coordinates $\mathbf{S}$ represent displacements from equilibrium positions:

$$\mathbf{S} = \boldsymbol{\zeta} - \boldsymbol{\zeta}_0 = \mathbf{L}_0 \bar{\mathbf{Q}} \tag{21}$$

and denoting with a prime one of the electronic states involved in the transition:

$$\boldsymbol{\zeta} = \boldsymbol{\zeta}_0 + \mathbf{L}_0 \bar{\mathbf{Q}} \tag{22}$$

$$\boldsymbol{\zeta} = \boldsymbol{\zeta}'_0 + \mathbf{L}'_0 \bar{\mathbf{Q}}'. \tag{23}$$

By Eqs. 22 and 23 and eliminating $\bar{\mathbf{Q}}$:

$$\begin{aligned} \bar{\mathbf{Q}} &= \mathbf{L}_0^{-1} \mathbf{L}'_0 \bar{\mathbf{Q}}' + \mathbf{L}_0^{-1} (\boldsymbol{\zeta}'_0 - \boldsymbol{\zeta}_0) \\ &= \mathbf{J}\bar{\mathbf{Q}}' + \mathbf{K}. \end{aligned} \tag{24}$$

3 Results

Several sets of internal coordinates for describing the vibrational motion of ammonia in both the neutral and the cationic $\tilde{X}^2A_2''$ state have been proposed [7, 16, 31–33]. We have adopted the set suggested by Hoy et al. [16] and developed by Handy and coworkers [7], which, although not orthogonal in the whole range of nuclear coordinates as that of Ref. [33], offers the advantage that the elements of the $\mathbf{G}$ matrix are already tabulated. It consists of the three N–H stretching coordinates (r_1, r_2, r_3), the angle (β) that each N-H bond forms with the trisector, that is, the axis forming the same angle with each bond vector, see Fig. 3, and any two of the three angles (α_i) obtained by projecting ammonia onto a plane perpendicular to the trisector. The adopted set of coordinate is shown in Fig. 3. Instead of r_1, r_2, r_3, we have used the symmetry adapted stretching coordinates R_1, R_2, R_3 defined as:

$$\begin{cases} R_1 = \frac{1}{\sqrt{3}}(r_1 + r_2 + r_3) \\ R_2 = \frac{1}{\sqrt{6}}(2r_1 - r_2 - r_3) \\ R_3 = \frac{1}{\sqrt{2}}(r_2 - r_3) \end{cases} \tag{25}$$

Harmonic vibrational frequencies and equilibrium geometries of the ground electronic states of NH_3 and NH_3^+ are reported in Table 1. They have been computed at two levels of computation in order to allow for comparison with both our previous FC computations [10] and with some of the high-level computations published up to now [34, 35]. The fourth order of the Møller Plesset perturbation theory, including single, double and quadruple excitations, in conjunction with the 6-311++G(3df,3pd) basis set (hereafter MP4/TZ) and the CCSD(T) method in conjunction with the aug-cc-pCVQZ core-valence basis set (hereafter CC/QZ) were used.

The $\mathbf{B}_0$ and $\mathbf{G}$ matrices have been evaluated following the procedure given in Ref. [7] and transformed according to Eq. 25. Analytical expressions of the elements of $\mathbf{G}$ are given in the Appendix. The coefficients g'_{rst} and g''_{rstu} appearing in the $\Delta\hat{T}$ term are reported in Table 2 both for MP4/TZ and for CC/QZ equilibrium geometries.

At the MP4/TZ level of approximation, the potential energy surface of NH_3^+ as a function of $\bar{Q}_1$ and $\bar{Q}_2$, the symmetric stretching and bending curvilinear normal coordinates, respectively, has been calculated over a grid of 431 points, covering the range $r_{\text{eq}} - 0.05\,\text{Å} \le r \le r_{\text{eq}} +$

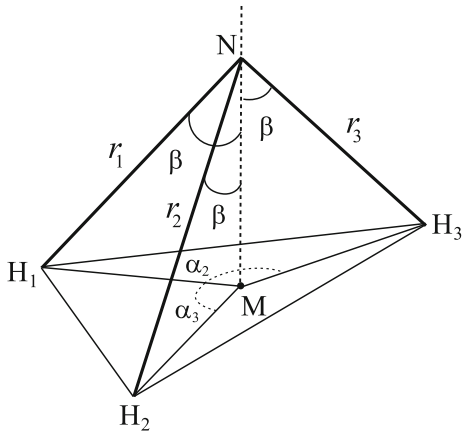

Fig. 3 Trisector axis (NM) at any nuclear configuration of ammonia: M belongs to the H_1–H_2–H_3 plane and is chosen in such a way that $\angle H_1NM = \angle H_2NM = \angle H_3NM = \beta$

Table 1 Predicted –MP4/TZ and CC/QZ– bond lengths (r_{eq}, Å), valence angles ∠HNH (θ_{eq}, degrees) and harmonic frequencies of the two symmetric modes ($\tilde{\nu}_i$ as wavenumbers, cm^{-1}) of NH_3 ($\tilde{X}^1A_1'$) and NH_3^+ ($\tilde{X}^2A_2''$)

	r_{eq}[a]	θ_{eq}	$\tilde{\nu}_1$[b]	$\tilde{\nu}_2$
MP4[c]				
$\tilde{X}^1A_1'$	1.0114	106.76	3523.94	1056.72
$\tilde{X}^2A_2''$	1.0203	120.00	3423.10	876.67
CC				
$\tilde{X}^1A_1'$	1.0115	106.71	3484.26	1053.01
$\tilde{X}^2A_2''$	1.0206	120.00	3376.51	865.87

[a] Experimental values are $r_{eq} = 1.0124$ Å, $\theta_{eq} = 106.67°$ for NH_3, Ref. [36], and $r_{eq} = 1.0145$ Å for NH_3^+, Ref. [37]

[b] Herzberg notation, $\tilde{\nu}_{1(2)}$ refers to symmetric stretching (bending)

[c] From Ref. [10]

Table 2 First-($uma^{-1/2}$ $Å^{-1}$) and second-order (uma^{-1} $Å^{-2}$) power expansion non-null coefficients of the kinetic energy of the $\tilde{X}^2A_2''$ electronic state of cationic ammonia

	MP4	CCSD(T)
g'_{212}	0.12170	0.12167
g'_{221}	−1.12732	−1.12703
g''_{2222}	−0.13720	−0.13713
g''_{2211}	1.90627	1.90530
g''_{2121}	−0.06860	−0.06856
g''_{1122}	0.16682	0.16674

1(2) is the symmetric stretching (bending)

0.05 Å and $\beta_{eq} - 10° \le \beta \le \beta_{eq} + 10°$. The potential energy has been fitted by different polynomials, one without coupling terms between the $\bar{Q}_1$ and the $\bar{Q}_2$ coordinates, the others with coupling terms having maximum order 4 in each variable. Since in the D_{3h} point group the totally symmetric stretching and the out-of-plane bending belong to different irreducible representations, all the terms in odd powers of $\bar{Q}_2$ are zero. The coefficients of the fitted polynomials are given in Table 3. It must be remarked that, in the case of MP4/TZ computations, we have deliberately chosen to use a small grid of points, much smaller than those used previously in the literature [10, 34, 35], in order to test the effectiveness of a good choice of internal curvilinear coordinates in relieving the computational efforts of computing anharmonic potential energy hypersurfaces for the calculation of FC factors. On the contrary, CC/QZ potential energy hypersurface has been calculated over a grid of 1,653 points, covering the range $0.9\,Å \le r \le 1.2\,Å$ and $88.6° \le \theta \le 120.0°$. The potential energy was fitted, in that case, by a polynomial of fourth degree in the dimensionless Morse variable:

Table 3 The coefficients of different polynomial fits of the MP4/TZ potential energy surface of the $\tilde{X}^2A_2''$ electronic state of cationic ammonia in terms of curvilinear normal coordinates (coefficients in $cm^{-1}/(amu^{1/2}\,Å)^n$, rms error in cm^{-1})

	P1	P2	P3
$\bar{Q}_2^2$	11319.66	11319.66	11318.95
$\bar{Q}_2^4$	11885.66	11886.66	11799.86
$\bar{Q}_1^2$	173774.00	173774.00	173766.66
$\bar{Q}_1^3$	−279077.51	−206229.84	−206229.85
$\bar{Q}_1^4$	161562.75	161562.75	152225.84
$\bar{Q}_1\bar{Q}_2^2$		−14873.10	−14873.09
$\bar{Q}_1^2\bar{Q}_2^2$			3196.46
rms error	22.2	0.3	0.2

$$\xi_1 = 1 - \exp(-a\bar{Q}_1),$$

and of 12th degree in $\bar{Q}_2$, with coupling terms up to 11th power:

$$V = \sum_{i=2}^{4} a_i \xi_1^i + \sum_{j=1}^{6} b_j \bar{Q}_2^{2j} + \sum_{k=1}^{4}\sum_{\ell=1}^{5} c_{k\ell}\xi_1^k \bar{Q}_2^{2\ell}; \quad k + 2\ell \le 11 \tag{26}$$

The coefficients of the fitted polynomial are given in Table 4.

The parameter a in ξ_1 was obtained by minimizing the RMS error of the monodimensional fit of the potential energy over the stretching coordinate (for $\theta = \theta_{eq}$) by using a potential of the form:

$$V_{str}(\bar{Q}_1) = \sum_{m=2}^{4} d_m[1 - \exp(-a\bar{Q}_1)]^m, \tag{27}$$

and was not re-optimized in the bidimensional fit.

The photoelectron spectrum of ammonia consists of two transitions, one corresponding to the removal of an electron from the HOMO, the nitrogen lone pair $3a_1$ orbital, the $\tilde{X}^2A_2'' \leftarrow \tilde{X}^1A_1'$ transition, the other corresponding to the removal of an electron from the 1e orbital, the $\tilde{X}^2E \leftarrow \tilde{X}^1A_1'$ transition. The ground-state electronic configuration is $1a_1^2 2a_1^2 1e^4 3a_1^2$ [4]. The $\tilde{X}^2A_2'' \leftarrow \tilde{X}^1A_1'$ lowest energy absorption exhibits a long vibrational progression, extending over about 2 eV and consisting of sixteen well-resolved vibrational peaks see Fig. 1 [5]. The highest intensities occur for the 7th and 8th peaks, whose intensity are nearly the same [5, 38], but the origin of the band at lowest energy is still uncertain, it could be either the $0 \leftarrow 0'$ transition (hereafter a prime will be used for the states of neutral ammonia) or a hot band. The observed vibrational spacing is *ca.* 0.12 eV (970 cm^{-1}), so that the long vibrational progression has been assigned to the ν_2 mode

Table 4 Parameters of the CC/QZ potential energy hypersurfaces of NH_3^+, Eq. 26

a_2	166968.647510294	c_{15}	−817.398711959657
a_3	−35289.0487979425	c_{21}	−1594.69984392527
a_4	11953.0683296960	c_{22}	−1951.90198081176
b_1	11121.4657867805	c_{23}	1191.88081069391
b_2	13245.5214498090	c_{24}	−258.787556100943
b_3	−7562.83554727964	c_{31}	3333.02647681526
b_4	5229.27984543509	c_{32}	−3721.84786330654
b_5	−2421.23199626368	c_{33}	21.1138010388612
b_6	547.255930418840	c_{34}	597.278450112574
c_{11}	−14062.5970311914	c_{41}	1044.63030334237
c_{12}	2027.23704747984	c_{42}	−1565.01400236844
c_{13}	−4463.71091704471	c_{43}	−401.619141894396
c_{14}	2826.24603526959	a	1.0063077647

Energy in cm^{-1}; ξ_1 dimensionless; $\bar{Q}_2$ in $uma^{1/2}$ Å; a in $uma^{-1/2}$ $Å^{-1}$, rms error = 0.1 cm^{-1}

(Herzberg's notation [39]), the so-called umbrella mode. In the high-resolution spectrum recorded by Edvardsson et al. [38], the strong progression due to the symmetric bending mode is accompanied by a much weaker but well-resolved one, falling at higher energy, which was tentatively assigned to the asymmetric bending mode with one more quantum on the symmetric bending mode.

As concerns neutral ammonia, a good representation of the two quasi-degenerate vibrational states is all we need for computing the photoelectron spectrum. A few test computations, carried out with an analytical anharmonic potential that reproduces the height of the inversion barrier (1,882 cm^{-1}), showed that the lowest energy states are well described by the symmetric and antisymmetric linear combinations of the two lowest energy vibrational states of each nuclear configuration, no significant contributions of higher-energy harmonic wavefunctions have been found. From the symmetric vibrational ground state, transitions to vibrational states with even quantum numbers are allowed, whereas states with odd quantum numbers are excited from the antisymmetric combination. Since the symmetric and antisymmetric vibrational modes of neutral ammonia are separated by only 0.79 cm^{-1} [32], Boltzmann populations of the two levels are equal and that allows to compute FC factors using only one equilibrium configuration of neutral ammonia. The initial state in all the FC calculations is therefore the harmonic ground vibrational state of the neutral molecule, the only one significantly populated at room temperature.

Among the six normal modes of the $\tilde{X}^2A_2''$ cationic state, only the symmetric stretching and the symmetric bending inversion modes play a role in the photoelectron spectrum if vibronic couplings are neglected [10, 38]. The stronger progression observed in the photoelectronic spectrum extends over an energy range of about 2 eV, so that a good representation of at least the lowest sixteen states associated with the inversion mode is needed. Thus, both potential anharmonic terms and the $\Delta\hat{T}$ kinetic terms are in principle important for this electronic state. Anharmonic wavefunctions of NH_3^+ have been computed by using the variational method, truncating the expansion of Eq. 16 to second order and neglecting the V_{kin} term, which is known to give very small contributions to the energies of the vibrational states [18, 19]. Forty harmonic oscillator basis functions for each mode centered in the minimum energy nuclear configuration of the cationic state have been used; that choice ensures convergence on the excited vibrational states in an energy region much larger than that of interest. Eigenstates have been computed by an implicitly restarted Arnoldi procedure. Analytical integrals have been used [15, 40, 41]. The computed energies of the vibrational states are reported in Table 5 together with the available experimental values [37, 42, 43]. Energies are predicted with reasonable accuracy by both the simple P1 potential of Table 3 and by the more accurate potential of Table 4; the latter one gives a significant improvement only for states with high quantum numbers on the v_2 mode. The agreement is not as good as that obtained by previous theoretical works [34], but it must be remarked that in the present work, the potential energy couplings of $\bar{Q}_1$ and $\bar{Q}_2$ with the other four normal coordinates have been neglected.

The $\tilde{X}^2A_2'' \leftarrow \tilde{X}^1A_1'$ photoelectronic spectrum of ammonia computed by considering the harmonic potential obtained at MP4/TZ level of computation, and the kinetic energy operator $\Delta\hat{T}$ of Eq. 16 is shown in Fig. 4.

Table 5 Computed and experimental energies (cm^{-1}) of the vibrational states of NH_3^+

Assignment	P1	CCSD(T)	Obs.[a]	Ref. [10]	Ref. [34]
$\tilde{\nu}_2$	918	908	903[b]	921	899
$2\tilde{\nu}_2$	1,874	1,854	1,844	1,873	1,837
$3\tilde{\nu}_2$	2,865	2,831	2,813	2,852	2,804
$\tilde{\nu}_1$	3,304	3,329	3,232[c]	3,373	3,231
$4\tilde{\nu}_2$	3,885	3,832	3,807	3,855	3,796
$\tilde{\nu}_1 + \tilde{\nu}_2$	4,221	4,231	4,127[c]	4,286	4,123
$5\tilde{\nu}_2$	4,931	4,855	4,821	4,878	4,809
$6\tilde{\nu}_2$	6,002	5,895	5,852	5,920	5,839
$\tilde{\nu}_1 + 3\tilde{\nu}_2$	6,165	6,140	6,022[c]	6,204	6,015
$7\tilde{\nu}_2$	7,093	6,952	6,899	6,979	6,885
$8\tilde{\nu}_2$	8,203	8,022	7,958	8,052	7,944
$9\tilde{\nu}_2$	9,331	9,104	9,030	9,139	9,015

[a] Ref. [42], except where otherwise noted

[b] Ref. [37]

[c] Ref. [43]

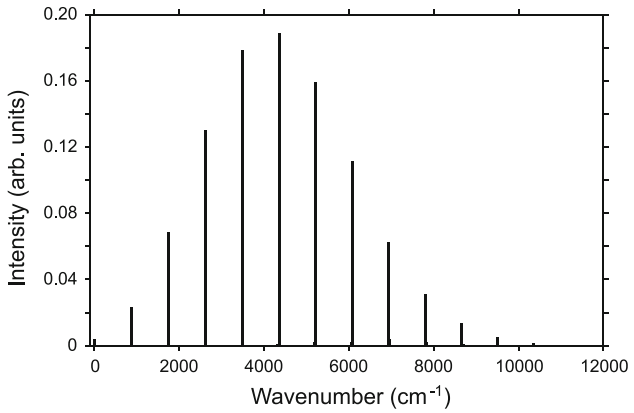

Fig. 4 Photoelectron spectrum of NH_3 computed using the MP4 harmonic potential and the kinetic energy operator $\Delta\hat{T}$

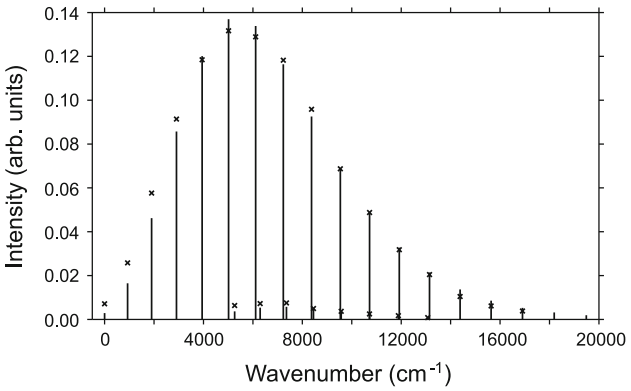

Fig. 5 Computed photoelectron spectrum of NH_3. *Verticle line* anharmonic potential P1 of Table 3, *Multiplication symbol* relative experimental intensities from Ref. [38]

Although the main features of the experimental spectrum are reproduced by FC computations, the predicted intensity distribution is significantly different from the observed one. The maximum peak height occurs for the $5 \leftarrow 0'$ transition, but the $6 \leftarrow 0'$ one exhibits a significantly lower intensity than the $5 \leftarrow 0'$ transition. More important discrepancies are observed in the high-wavenumber region, where the relative intensities of the computed spectrum decay much faster than the experimental ones. The intensities of the higher-energy transitions are significantly underestimated, and therefore, the spectrum exhibits only 13 peaks, whereas in the experimental one at least 16 peaks are clearly observed. The results obtained by using a harmonic potential are thus in many aspects similar to those previously obtained by employing the internal coordinate representation but using a simplified expression of $\hat{T}$, without including the $\Delta\hat{T}$ terms [10, 44]. Indeed, the $\Delta\hat{T}$ kinetic operator only provides corrections of a few tens of cm^{-1} on the computed energies, without significantly affecting the computed eigenvectors.

The computed spectrum obtained by using the P1 anharmonic potential of Table 3 together with kinetic $\Delta\hat{T}$ is shown in Fig. 5 and compared with the experimental intensities of Ref. [38]. The latter ones have been obtained from the peak areas of the deconvoluted photoelectron spectrum, which have been then normalized to unity for comparison with the theoretical one. The whole spectrum is well reproduced, especially as concerns its decay in the longer-wavenumber region, which had posed problems in previous theoretical investigations [12]. The experimental bandwidth is also well reproduced by FC calculations; Rabelais' experimental spectrum shows sixteen well-resolved peaks, with a little not resolved tail, whereas the theoretical one exhibits one more. The computed spectrum also shows the presence of a second much weaker progression, which the calculation assigns to transitions to vibrational states with excitations on the bending mode v_2 and a single quantum on the totally symmetric stretching mode v_1, in agreement with previous theoretical results [10, 13, 14]. The weaker progression is very well resolved in the high-resolution spectrum of Edvardsson et al. [38] who tentatively assigned it to transitions to a vibrational progression of the asymmetric bending mode with one more quantum on the symmetric bending mode v_2. The asymmetric bending mode is of E symmetry, and therefore, vibronic couplings should be invoked to justify the presence of such combination bands in the experimental spectrum. In the experimental spectrum, the weak progression starts just after the sixth peak of the stronger progression, about 5,400 cm^{-1} after the $0 \leftarrow 0'$ transition and exhibits a maximum for the third peak. In the computed spectrum the weak progression starts after the fifth peak and the maximum peak height falls at the forth peak. The adopted scaling was the same as for the main progression; thus, the good agreement between the relative intensities of the weak and the strong progression further supports our assignment.

The computed spectra obtained by using the other potential energy functions of Table 3 are very similar to that obtained by using the simplest P1 potential as concerns the stronger progression; a slight detriment on the intensities and width of the weaker progression is observed when couplings between $\bar{Q}_1$ and $\bar{Q}_2$ are introduced in the potential energy expressions, possibly because of the small grid used in the electronic calculations, not sufficiently large, especially for the totally symmetric stretching mode, to provide the coupling terms with the required accuracy for calculations of the FC factors.

The deviation from the experimental relative intensities is more pronounced for low-energy levels, whereas the high region of the spectrum is better reproduced. That unexpected behavior—the quality of the computed states at low energy should be higher than those at higher energy—can be due to the presence of overlapping bands in the

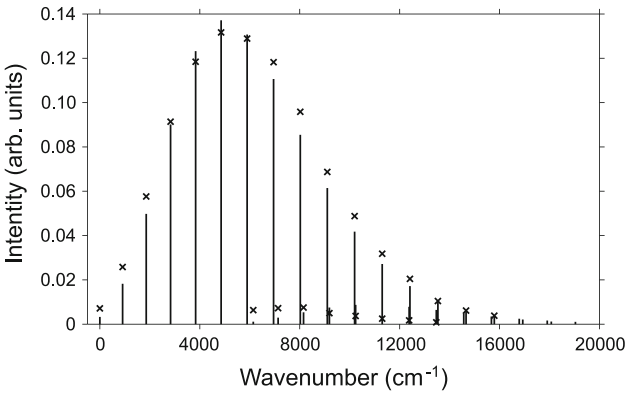

Fig. 6 Computed photoelectronic spectrum of NH_3. *Verticle line* anharmonic potential of Table 4, *Multiplication symbol* relative experimental intensities from Ref. [38]

experimental spectrum, which makes the estimation of FC factors by the deconvolution technique difficult. Indeed, on the assumption that the first observed band is a hot band, as experimental and theoretical evidence leads to suppose [13, 38], a possible explanation of the low intensity is that other peaks of the hot progression could be hidden under the lower-energy peaks. Indeed previous calculations of FC factors from the $|0'1'\rangle$ state of neutral ammonia indicates that the transition $00 \leftarrow 0'1'$ is not the most intense one, but it should be accompanied by at least four transitions of the type $0n \leftarrow 0'1'$ $(n = 1, 2, \ldots)$, which have still higher intensities [10]. Actually FC computations yield a quite long progression for the hot band with relative intensities 0.02, 0.08, 0.14, 0.13 and 0.05 for $n = 0$, 1, 2, 3 and 4, respectively. Those hot transitions could affect the intensities of the peaks of the main progression making the comparison of the computed and the observed spectrum even more difficult.

The spectrum obtained by using the CC/QZ potential energy of Table 4 is shown in Fig. 6. It is quite similar to that obtained by using the simplest P1 potential, exhibiting a slight improvement in the low-energy region of the spectrum, but to detriment of the middle energy region, and of the second less intense progression, which, within the limits of the deconvolution procedure used by us for assigning experimental intensities, is slightly longer than the observed one.

4 Conclusion

Prediction of the band shapes for radiative transitions between electronic states with significantly different minimum energy nuclear configurations along an angular coordinate (floppy molecules) requires caution. Gribov's definition of curvilinear normal coordinates allows the generalization of Duschinsky's transformation to the case of curvilinear coordinates. Those coordinates can be extremely useful for floppy molecules, inasmuch they could allow for decoupling the displaced modes, making it easier the computation of the potential energy hypersurface. Here we have shown that the photoelectron spectrum of ammonia, the prototype of floppy molecules, can be reproduced with sufficient accuracy, by using the curvilinear internal coordinate representation of the normal modes of the neutral and ionic state, providing that anharmonic potential energy terms for the two coordinates that play the dominant role in the photoelectron spectrum are properly included. The treatment of anharmonic effects at the full six-dimensional level does not appear to be necessary, although high accuracy on vibrational frequencies, comparable to that of previous work [34], cannot be obtained within the two-dimensional anharmonic model adopted here. The computational effort for the characterization of anharmonic potential energy terms is significantly relieved by using curvilinear coordinates, both because in the case of ammonia curvilinear coordinates allows for decoupling the two active modes with a good accuracy, and because of the limited number of electronic computations to be carried out for the characterization of the potential energy hypersurface. Indeed in the Cartesian coordinate representation, a grid of about 4300 points, covering the range $0.57\,\text{Å} \leq r \leq 1.65\,\text{Å}$ and $40° \leq \theta \leq 120°$, was necessary for obtaining reasonable results, whereas in the present work, a much smaller grid of 431 points, covering the range $r_{eq} - 0.05\,\text{Å} \leq r \leq r_{eq} + 0.05\,\text{Å}$ and $\beta_{eq} - 10° \leq \beta \leq \beta_{eq} + 10°$, has been sufficient. In the case of ammonia, probably because of the good choice of internal coordinates, the dependence of the **G** matrix terms upon the curvilinear coordinates plays a minor role, it can be neglected if a high accuracy on frequencies is not required.

5 Computational details

Equilibrium geometries, harmonic frequencies and Cartesian normal coordinates for NH_3 and NH_3^+ were computed by using the CFOUR program at both MP4 and CCSD(T) levels [45]. The unrestricted formalism was used for NH_3^+. All the electrons –included core 1s of nitrogen– were explicitly correlated both in CCSD(T) and MP4 computations. The MP4 potential energy surface of NH_3^+ was computed at the UMP4(SDQ)/6-311++G(3df,3pd) level by using the Gaussian package [46]. The CCSD(T) potential energy surface of NH_3^+ has been calculated by using the Molpro suite of programs [47]. The UCCSD(T) level of theory in conjunction with the aug-cc-pCVQZ core-valence basis set was used. Franck–Condon

factor computations were carried out by using a development version of the MolFC package [48–50].

Acknowledgments The financial support of the University of Salerno is gratefully acknowledged.

Appendix: The G matrix

In the following:

$$\alpha_1 = 2\pi - \alpha_2 - \alpha_3; \tag{28}$$

$$\psi_i = \frac{\alpha_i}{2}; \quad i = 1,2,3; \tag{29}$$

$$\mu = \frac{m_N m_H}{m_N + m_H}. \tag{30}$$

$$\begin{aligned} G_{\beta\beta} = & \frac{\cos^2\psi_1}{4\mu(\sin^2\psi_2)(\sin^2\psi_3)\left(\frac{R_1}{\sqrt{3}}+\frac{2R_2}{\sqrt{6}}\right)^2} \\ & + \frac{\cos^2\psi_2}{4\mu(\sin^2\psi_1)(\sin^2\psi_3)\left(\frac{R_1}{\sqrt{3}}-\frac{R_2}{\sqrt{6}}+\frac{R_3}{\sqrt{2}}\right)^2} \\ & + \frac{\cos^2\psi_3}{4\mu(\sin^2\psi_1)(\sin^2\psi_2)\left(\frac{R_2}{\sqrt{6}}-\frac{R_1}{\sqrt{3}}+\frac{R_3}{\sqrt{2}}\right)^2} \\ & + \frac{(\cot\psi_2)(\cot\psi_3)\left[2(\sin^2\psi_1)(\cos^2\beta)-1\right]}{2m_N(\sin^2\psi_1)\left(\frac{R_2}{\sqrt{6}}-\frac{R_1}{\sqrt{3}}+\frac{R_3}{\sqrt{2}}\right)\left(\frac{R_1}{\sqrt{3}}-\frac{R_2}{\sqrt{6}}+\frac{R_3}{\sqrt{2}}\right)} \\ & + \frac{(\cot\psi_1)(\cot\psi_2)\left[2(\sin^2\psi_3)(\cos^2\beta)-1\right]}{2m_N(\sin^2\psi_3)\left(\frac{R_1}{\sqrt{3}}+\frac{2R_2}{\sqrt{6}}\right)\left(\frac{R_2}{\sqrt{6}}-\frac{R_1}{\sqrt{3}}-\frac{R_3}{\sqrt{2}}\right)} \\ & + \frac{(\cot\psi_1)(\cot\psi_3)\left[2(\sin^2\psi_2)(\cos^2\beta)-1\right]}{2m_N(\sin^2\psi_2)\left(\frac{R_1}{\sqrt{3}}+\frac{2R_2}{\sqrt{6}}\right)\left(\frac{R_2}{\sqrt{6}}-\frac{R_1}{\sqrt{3}}+\frac{R_3}{\sqrt{2}}\right)} \end{aligned} \tag{31}$$

$$G_{R_1R_1} = \frac{1}{\mu} - \frac{4\sin^2\beta(\sin^2\psi_1+\sin^2\psi_2+\sin^2\psi_3)-6}{3m_N} \tag{32}$$

$$\begin{aligned} G_{\beta R_1} = & \frac{\sqrt{3}\sin(2\beta)}{6m_N\sin\psi_2}\left(\frac{\cos\psi_3\sin\psi_1}{\frac{R_2}{\sqrt{6}}-\frac{R_1}{\sqrt{3}}+\frac{R_3}{\sqrt{2}}}-\frac{\cos\psi_1\sin\psi_3}{\frac{R_1}{\sqrt{3}}+\frac{2R_2}{\sqrt{6}}}\right) \\ & - \frac{\sqrt{3}\sin(2\beta)}{6m_N\sin\psi_3}\left(\frac{\cos\psi_1\sin\psi_2}{\frac{R_1}{\sqrt{3}}+\frac{2R_2}{\sqrt{6}}}+\frac{\cos\psi_2\sin\psi_1}{\frac{R_1}{\sqrt{3}}-\frac{R_2}{\sqrt{6}}+\frac{R_3}{\sqrt{2}}}\right) \\ & - \frac{\sqrt{3}\sin(2\beta)}{6m_N\sin\psi_1}\left(\frac{\cos\psi_2\sin\psi_3}{\frac{R_1}{\sqrt{3}}-\frac{R_2}{\sqrt{6}}+\frac{R_3}{\sqrt{2}}}-\frac{\cos\psi_3\sin\psi_2}{\frac{R_2}{\sqrt{6}}-\frac{R_1}{\sqrt{3}}+\frac{R_3}{\sqrt{2}}}\right) \end{aligned} \tag{33}$$

References

1. Walsh AD, Warsop PA (1961) Trans Faraday Soc 57:345
2. Douglas AE (1963) Discuss Faraday Soc 35:158
3. Branton GR, Frost DC, Herring FG, McDowell CA, Stenhouse LA (1969) Chem Phys Lett 3:581
4. Weiss MJ, Lawrence GM (1970) J Chem Phys 53:214
5. Rabalais JW, Karlsson L, Werme LO, Bergmark T, Siegbahn K (1973) J Chem Phys 58:3370
6. Leonard C, Handy NC, Carter S, Bowman JM (2002) Spectrochim Acta A 58:825
7. Handy NC, Carter S, Colwell SM (1999) Mol Phys 96:477
8. Reimers JR (2001) J Chem Phys 115:9103
9. Borrelli R, Peluso A (2006) J Chem Phys 125:194308
10. Peluso A, Borrelli R, Capobianco A (2009) J Phys Chem A 113:14831
11. Domcke W, Cederbaum LS, Köppel H, Von Niessen W (1977) Mol Phys 34:1759
12. Ågren H, Reineck I, Veenhuizen H, Maripuu R, Arneberg R, Karlsson L (1982) Mol Phys 45:477
13. Viel A, Eisfeld W, Neumann S, Domcke W, Manthe U (2006) J Chem Phys 124:214306
14. Viel A, Eisfeld W, Evenhuis CR, Manthe U (2008) Chem Phys 347:331
15. Wilson EBJ, Decius JC, Cross PC (1955) Molcular vibrations. McGraw Hill, New York
16. Hoy AR, Mills IM, Strey G (1972) Mol Phys 24:1265
17. Kuchitsu K, Morino Y (1965) Bull Chem Soc Japn 38:805
18. Sibert EL, Hynes JT, Reinhardt WP (1983) J Phys Chem 87:2032
19. Gribov LA, Orville-Thomas W (1988) Theory and methods of calculation of molecular spectra. Wiley, Chichester
20. Gribov LA (1992) J Struct Chem (Engl. Transl.) 33:478
21. Villaseñor-González P, Cisneros-Parra J (1981) Am J Phys 49:754
22. Nauts A, Chapuisat X (1985) Mol Phys 55:1287
23. Gribov LA (1970) Opt Spectrosc 30:1247
24. Pavlyuchko AI, Gribov LA (1983) Opt Spectrosc 54:644
25. Seidner L, Stock G, Sobolewski AL, Domcke W (1992) J Chem Phys 96:5298
26. Isaacson AD (2006) J Phys Chem A 110:379
27. Cederbaum LS, Domcke W (1976) J Chem Phys 64:603
28. Cederbaum LS, Domcke W (1976) J Chem Phys 64:612
29. Quade CR (1976) J Chem Phys 64:2783 (See also erratum *ibid.* 79, 4089 (1983))
30. Dushinsky F (1937) Acta Physicochim. URSS 7:551
31. Špirko V (1983) J Mol Spectrosc 101:30
32. Špirko V, Kraemer WP (1989) J Mol Spectrosc 133:331
33. Ragni M, Lombardi A, Pereira Barreto PR, Peixoto Bitencourt AC (2009) J Phys Chem A 113:15355
34. Yurchenko SN, Thiel W, Carvajal M, Jensen P (2008) Chem Phys 346:146
35. Léonard C, Carter S, Handy NC (2002) Phys Chem Chem Phys 4:4087
36. Morino Y, Kuchitsu K, Yamamoto S (1968) Spectrochim Acta A 24:335
37. Lee SS, Oka TT (1991) J Chem Phys 94:1698
38. Edvardsson D, Baltzer P, Karlsson L, Wannberg B, Holland DMP, Shaw DA, Rennie EE (1999) J Phys B 32:2583
39. Herzberg G (1945) Infrared and raman spectra of polyatomic molecules. Van Nostrand Co. Inc., Princeton, NJ
40. Califano S (1976) Vibrational states. Wiley, New York
41. Morales J, Palma A, Sandoval L (1986) Int J Quantum Chem 29:211
42. Reiser G, Habenicht W, Müller-Dethlefs K (1993) J Chem Phys 98:8462
43. Bahng MK, Xing X, Baek SJ, Ng CY (2005) J Chem Phys 123:084311
44. Harshbarger WR (1970) J Chem Phys 53:903
45. CFOUR, a quantum chemical program package written by Stanton JF, Gauss J, Harding ME, Szalay PG with contributions from Auer AA, Bartlett RJ, Benedikt U, Berger C, Bernholdt DE, Bomble YJ, Christiansen O, Heckert M, Heun O, Huber C, Jagau

T-C, Jonsson D, Jusélius J, Klein K, Lauderdale WJ, Matthews DA, Metzroth T, O'Neill DP, Price DR, Prochnow E, Ruud K, Schiffmann F, Stopkowicz S, Tajti A, Vázquez J, Wang F, Watts JD and the integral packages MOLECULE (Almlöf J and Taylor PR), PROPS (Taylor PR), ABACUS (Helgaker T, Jensen HJ Aa, Jørgensen P, and Olsen J), and ECP routines by Mitin AV, van Wüllen C. For the current version, see http://www.cfour.de

46. Frisch MJ, Trucks GW, Schlegel HB, Scuseria GE, Robb MA, Cheeseman JR, Scalmani G, Barone V, Mennucci B, Petersson GA, Nakatsuji H, Caricato M, Li X, Hratchian HP, Izmaylov AF, Bloino J, Zheng G, Sonnenberg JL, Hada M, Ehara M, Toyota K, Fukuda R, Hasegawa J, Ishida M, Nakajima T, Honda Y, Kitao O, Nakai H, Vreven T, Montgomery JA Jr., Peralta JE, Ogliaro F, Bearpark M, Heyd JJ, Brothers E, Kudin KN, Staroverov VN, Kobayashi R, Normand J, Raghavachari K, Rendell A, Burant JC, Iyengar SS, Tomasi J, Cossi M, Rega N, Millam JM, Klene M, Knox JE, Cross JB, Bakken V, Adamo C, Jaramillo J, Gomperts R, Stratmann RE, Yazyev O, Austin AJ, Cammi R, Pomelli C, Ochterski JW, Martin RL, Morokuma K, Zakrzewski VG, Voth GA, Salvador P, Dannenberg JJ, Dapprich S, Daniels AD, Farkas, Foresman JB, Ortiz JV, Cioslowski J, Fox DJ (2009) Gaussian 09 revision A.02. Gaussian Inc. Wallingford, CT
47. Werner HJ, Knowles PJ, Knizia G, Manby FR, Schütz M, Celani P, Korona T, Lindh R, Mitrushenkov A, Rauhut G, Shamasundar KR, Adler TB, Amos RD, Bernhardsson A, Berning A, Cooper DL, Deegan MJO, Dobbyn AJ, Eckert F, Goll E, Hampel C, Hesselmann A, Hetzer G, Hrenar T, Jansen G, Köppl C, Liu Y, Lloyd AW, Mata RA, May AJ, McNicholas SJ, Meyer W, Mura ME, Nicklass A, O'Neill DP, Palmieri P, Pflüger K, Pitzer R, Reiher M, Shiozaki T, Stoll H, Stone AJ, Tarroni R, Thorsteinsson T, Wang M, Wolf A (2010) Molpro, version 2010.1, a package of ab initio programs. See http://www.molpro.net
48. Peluso A, Santoro F, Del Re G (1997) Int J Quantum Chem 63:233
49. Borrelli R, Peluso A (2003) J Chem Phys 119:8437
50. Borrelli R, Peluso A. MolFC: a program for Franck-Condon integrals calculation. Package available online at http://www.theochem.unisa.it